Advanced Ceramics Progress

Research Article

Journal Homepage: www.acerp.ir

An investigation on Mechanical Properties of Apatite-Wollastonite-Diopside Glass-Ceramics Composites

A. Faeghinia*, E. Salahi

Ceramic Division, Materials and Energy Research Centre, P. O. Box: 14155-4777, Tehran, Iran

PAPER INFO

Paper history:
Received 06 November 2017
Accepted in revised form 31 October 2018

Keywords:
Pressureless Sintering
Mechanical properties
Relative Density
Hardness
Ceramic Composite

ABSTRACT

In the present study, Apatite-Wollastonite-Diopside glass-ceramic composites were prepared by the pressureless sintering process at the temperature range of 1100-1160 ºC. The weight percentage of phlogopite was varied between 10% and 50%. In addition, the bending strengths were increased from 100 to 170 Mpa by increasing the content of phlogopite up to 20 wt%. Furthermore, the sintering conditions were studied via characterizing the linear shrinkages and the relative densities of sintered samples. The relative density of composites increased through increasing the content of phlogopite up to 83% at 1050 ºC in C55 sample (with 50:50 weight percent). The XRD results showed that the forsterite as well as the phlogopite phase caused the maximum hardness of 16 GPa in C28 sample .

1. INTRODUCTION

Glass-ceramic apatite–wollastonite (A–W) [1] is a bioactive ceramic which can promote bone regeneration and provide strong interfacial bonding between the implant and host tissue in areas such as iliac crest and spine [2-4]. The presence of crystalline apatite ($Ca_{10}(PO_4)_6(O, F_2)$) and wollastonite ($CaO{\cdot}SiO_2$) in a MgO–CaO–SiO_2 glassy matrix lead to that the A–W glass-ceramic possesses greater tensile strength than both bioglass® and sintered hydroxyapatite (HA) [5-8] as well as human cortical bone [9]. These phases can be maintained for a longer period in the body environment, making it a highly desirable implant material [10, 11]. Despite having desirable mechanical strength, high elastic modulus, the ceramic materials are prone to low fracture toughness. Considering their utilities, several research works therefore have been carried out to improve the fracture toughness of these glass ceramics.
Texturing has been conducted by extrusion of apatite glass-ceramics [12] in order to enhance the fracture toughness. Some other researchers, however, have proposed applying ZrO_2 as a reinforcement into the A-W glass-ceramics [13]. They reported the numbers of 480 MPa and 2.6MPa.m1/2 for bending strength and fracture toughness, respectively, in the case of glass-ceramics containing 50% zirconia. for, Cooper [14] has investigated the potential of using phlogopite glass as a fiber/ceramic–matrix composite. According to his research, phologopite interface was sufficiently weak to provide debonding and crack deflection. The fiber reinforced ceramic matrix composite exhibited non-catastrophic fracture behavior during the fiber extensive pullout. Therefore, it is expected that the fine mica particles, precipitated at the inter granular region, would heighten the fracture toughness or the machinability of the composites [15].On the other hand, it has been proved that some glasses, which may be produced by mixing powders of different glasses, meet the properties changing of the original glasses [16].
The present work is another attempt to improve the properties of A-W glass-ceramics by means of their mixing with phlogopite glass composition.

2. EXPERIMENTAL PROCEDURE

2.1. Glass melting

Apatite-wollastonite (A-W) [1] and phlogopite (Ph) glasses [21] were prepared by applying several reagents-grade $MgCO_3$ (Merck ArtNo. 5828, Germany), K_2CO_3 (Merck Art No. 7734, Germany), MgF_2, (Merck Art No 7783, 6-40, Germany) $H_2[PO_4]_3$, Al_2O_3 and SiO_2

*Corresponding Author's Email: Aida.faeghinia@gmail.com (A.Faeghinia)

sand, while the batches were calcinated at 900ºC for 24 hrs. During the initial experiments indicated in Tables 1 and 2, the nominal and analytical compositions of different glasses were studied. The A-W and Ph glass compositions were melted at 1450°C and 1550 °C, respectively, which were kept in an electric furnace for 2 hrs using Pt crucibles. In order to obtain frits, these melts were poured into the cold water.

TABLE 1. Nominal/analyzed composition of AW glass(wt.%)

O_2		P_2O_5		CaO		F		MgO	
32	34.2	16.3	14	47	44.9	0.20	0.5	3.54	4.6

TABLE 2. Nominal/analyzed composition of ph glass (wt. %)

SiO_2		Al_2O_3		B_2O_3		K_2O		F		MgO	
40	40.2	14	14.6	12	12.4	6	6.57	14	7.80	18	17.9

2.2. Particle size distribution

In the next step, dry frits were grounded using an agate mill and sieved with a 60-µm mesh. The particle size distribution of glass powders was determined using laser scattering with a Mastersizer S instrument [Malvern Instruments]. Figure 1 shows the PSA analysis of the two frites. The results of D_{50} and specific surface area are presented in Table 3. It is worthy to mention that these two glasses were mixed together to make a composite. Moreover, all melted glasses displayed a broad amorphous XRD profile.

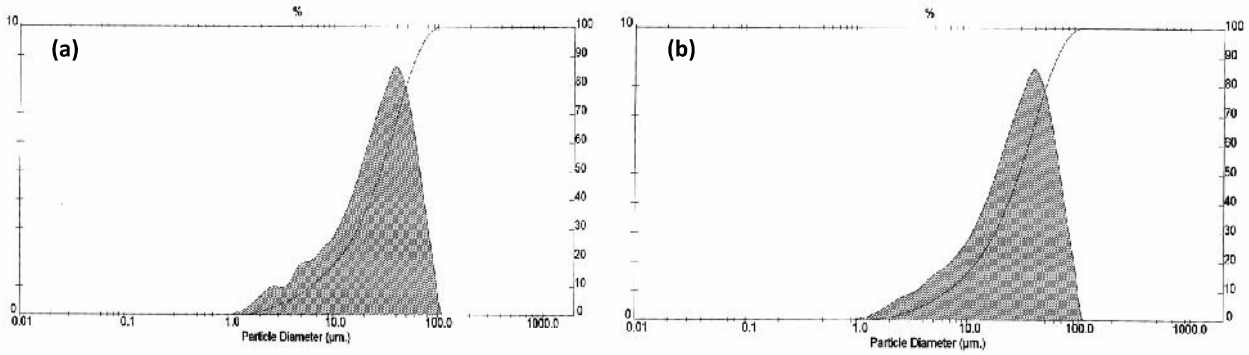

Figure 1. Particle size distribution of (a) A-W frits and (b) ph frits

TABLE 3. Specific surface area and density of obtained frits

Samples	Density (g/cm^3)	Specific surface area
Ph	2.55	0.23
A/W	2.91	0.20

2.3. Preparation of composites

Mixtures were prepared by combining matrix (A-W) and Ph glasses with different ratios (5 to 50 wt. %) in acetone solution. Then it was shacked in a tubule mixer for 1 hand dried in an oven at 60ºC. Table 4 shows the four specimens of the composites through 1:9, 2:8, 3:7 and 5:5 weight ratio denoted by C19, C28, C37 and C55, respectively. All of these specimens as small green plates were treated isothermally at 1100°C, 1120°C, 1140°C and 1160°C, correspondingly, for almost 60 min. the optimum of heat treatment region was measured by obtaining the minimum values of open porosity and the maximum values of linear shrinkage in order to acquire dense composites.

TABLE 4. The composition of different composites

Composite	Ph glass (wt. %)	A/W glass (wt. %)
C19	10%	90%
C28	20%	80%
C37	30%	70%
C55	50%	50%

2.4. Mechanical properties analysis

Hardness was determined by means of samples polished down to a 1 µm finish using diamond-paste. A Vickers indent load of 1 kg.f was then applied to the polished surface through Micromet 3 micro-hardness testers (Buehler LTD, Lake Bluff, IL, USA) with a 30 sec. dwell time. It can be calculated according to the Eq. (1):

$$H = \frac{P}{\alpha a^2} \quad (1)$$

Where α=2 and a is the half diagonal of the indent [17]. Ten samples from each type of composite were selected to perform a three-point bend testing. The specimens were shaped and then polished using 8 µm silicon carbide papers to reach a sample with 3 mm×4mm×40mm size To apply a load over a 30 mm span, at the mid-point of the surface, Instron testing machine was utilized. All tests were fulfilled at ambient temperature using a cross-head speed of 0.5 mm/min and. The values for bending strength and Young's modulus at failure point were calculated based on the equations (2) and (3), respectively [17]:

$$\delta_f = \frac{3P_f L}{2bh^2} \quad (2)$$

$$E = \frac{\delta}{\varepsilon} \quad (3)$$

Where $\sigma=3PL/2bh^2$ and $\varepsilon_e=6\ h\ \delta/\ L^2$. P denotes the load at the elastic limit (N), P_f is the load at fracture point (N), L is the sample length (mm), δ is the displacement of crosshead (mm), b is the sample breadth (mm) and h is the sample height (mm).In a same mechanical test, fracture toughness was determined for glass-ceramics through indentation strength. The indentation toughness equation was developed by Chantikul *et. al.* [17] shown in the following:

$$K_C = \zeta_z \left(\frac{E}{H}\right)^{\frac{1}{8}} \left(\delta_f P^{\frac{1}{3}}\right)^{\frac{3}{4}} \quad (4)$$

Where K_c is the toughness, E is the elastic modulus, P is the indentation load, H is the hardness, σ_f is the applied stress at fracture point and ζ_z is an empirical constant (0.59±0.12).

3. RESULTS AND DISCUSSION

In order to evaluate the sintering process, the linear shrinkages of the composites were measured via applying a 10 °C/min heating rate At that time, green samples were treated isothermally at 1100 °C, 1120 °C, 1140 °C and 1160 °C for 60 minutes. Figure 2 shows the linear shrinkage of composites versus temperature. Table 5 also depicts the relative densities and sintering temperatures of the composites.

The results also indicated that the maximum densification of composites was in the temperature range of 1140-1180 °C, which were evidently very close to their melting temperatures. The given interval sintering temperature was positioned certainly higher than the sintering temperatures that have been found for A-W (Apatite-Wollastonite) and (Phlogopite) individual glasses before[1,2].

The delay in densification may be due to the crystallization or reaction between the components of the two glasses [13]. On the other hand, if the effective crystalline phases in the composites vary based on the temperature, one will be might expect additional changes in the sintering trend compared to a single (constant) composition. Otherwise, the low relative density of the heat-treated composites at the sintering temperature may be attributed to the effect of secondary porosity, which is more pronounced in the higher temperature heat treatment [13]. Figure 3 shows the evolution of the phases over the sintered samples. The sintered composites exhibit similar crystalline phases, which should be essentially apatite, wollastonite, diopside and forsterite.

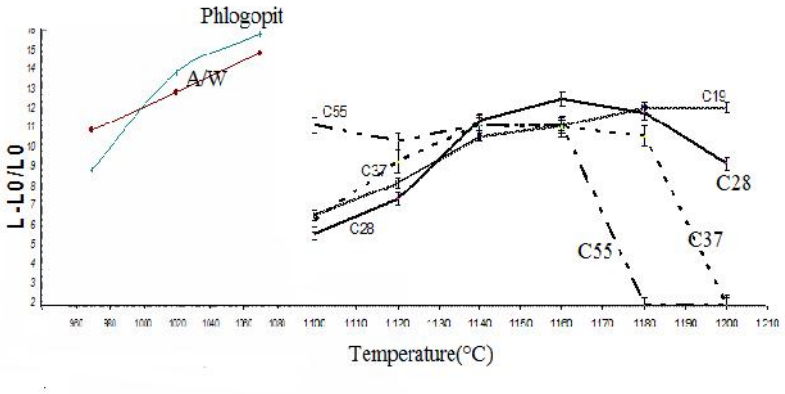

Figure 2. Linear shrinkage of the composites

TABLE 5. Maximum sintering melting temperature and relative densities of the composites

Samples	C19	C28	C37	C55	A-W glass	Ph glass
Sintering temperature °C	1180	1160	1140	1050	1080	1060
Melting temperature °C	1200	1180	1150	1070	-	-
Relative density g/cm^3	75%	87%	79%	83%	95%	79%

In addition, the XRD patterns showed an almost complete disappearance of the phlogopite phase (this phase has been realized in the previous study [21]). It is assumed that the diopside phase is formed in all sintered composites because of the dissolved phlogopite.

Diopsidic pyroxene as a major phase is formed due to the wide limits of isomorphous substitutions in the pyroxene formula. There is a possibility for contribution of $CaAl_2SiO_6$ Molecules in the building of pyroxene

structure with aluminum ions that occupy fourth and sixth coordination positions to form complex aluminous pyroxene solid solutions under the non-equilibrium conditions.

By increasing the temperature, phlogopite crystals probably dissolve and infiltrate MgO content into the residual glass, which most likely facilitate the diopside formation. On the other hand, the forsterite phases forme as a result of fluor volatilization and re-dissolution of the phlogopite crystals [14]. However, these were not identified in the C28 sample in comparison with the other composites.

Moreover, the recognized weak peaks of melilite in the C55 sample and the lower proportion of the crystalline phases (according to the XRD patterns) indicate a more amorphous phase in this case.

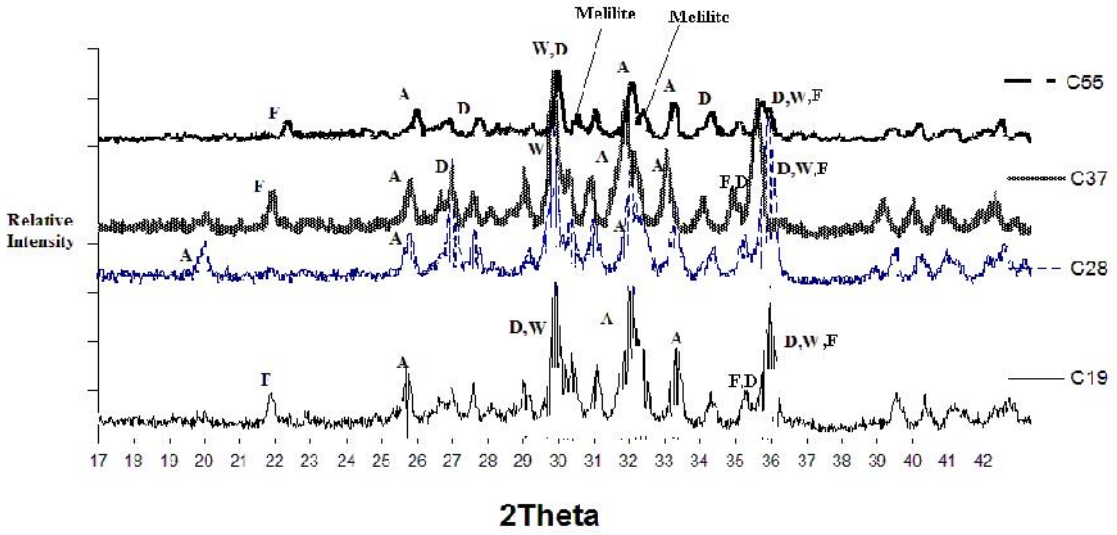

Figure 3. XRD patterns of composites isothermally- heat-treated at the sintering

Similar to the previous research [15], the evaporation of fluor from the phlogopite glass composition has an important role in the reaction and sintering process. Figure 4 shows the gradual weight loss of the composites at the appropriate sintering temperature.

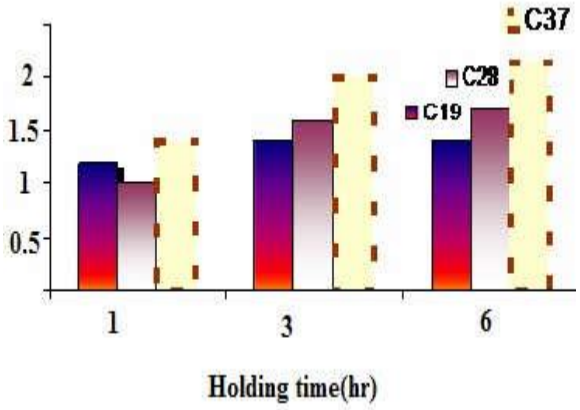

Figure 4. The weight loss of the composites in their sintering temperatures

The observed weight losses are due to the evaporation of H_2O, CO, CO_2, fluor and boron [15]. According to the weight loss results (Figure 4), it is apparent that weight loss enhance markedly in the composites with more Ph glass quantity using the optimum holding-time at the sintering temperature. Furthermore, phlogopite dissolution can be explained by Figure 4.

3.1 Mechanical properties analysis

Figure 5 shows the values of three-point bending strength and Young's modulus of the composites as a function of phlogopite content after sintering process at the optimum temperature.

Since the bending strength highly dependes on the relative density and according to the high density of C28 sample, it should be unsurprisingly mentioned to its higher mechanical properties including bending strength and Young's modulus than the other composites.

Furthermore, low strength of the C55 sample can be explained established upon its number of crystalline phases, which are lower than the other samples.

Figure 6 shows the results of microhardness and fracture toughness.

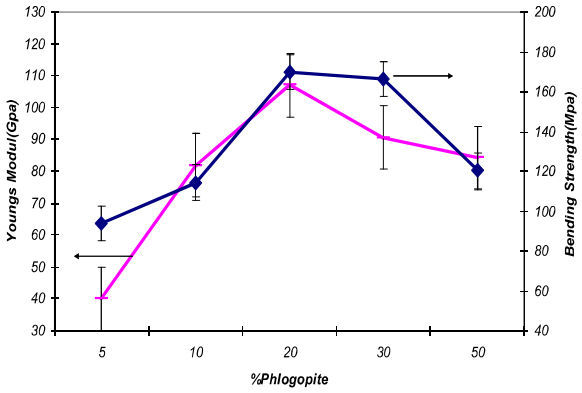

Figure 5. Three-point bending strength and Young's module of the composites

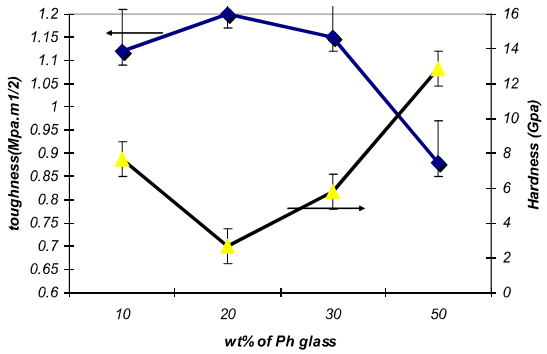

Figure 6. The results of microhardness and fracture toughness of the composites

TABLE 6. The mechanical properties results of the composites

Sample	Bending Strength (Mpa)	Young's Modules	Micro Hardness (Gpa)	Fracture Toughness (Mpa.m$^{1/2}$)
C19	81.95257	114.38	7.66	1.12
C28	107.02	170	2.65	1.2
C37	90.54813	166.41	5.81	1.15
C55	84.30151	120.36	12.84	0.88
C19	81.95257	114.38	7.66	1.12

Forsterite is known because of its optimum hardness (7 Mohs). Since forsterite was not detected in the C28 sample, its hardness is significantly lower than the other composites. A strong correlation between the content of forsterite and the hardness are shown in Table 6.
The microstructures of the C55 and C28 samples are compared in figures 7 and 8. According to the EDS analyses, the observed particles were diopside.

3.2 Microstructural characterization

For the heat-treated C55 sample at 1050 ºC and a 1 hour holding-time, a few isolated crystals were formed and a slight melting of the sample was observed. The heat treatment on the sample caused melting the crystalline phases and led to an uneven rough surface texture. Figure 9 depicts the precipitated higher volume fraction of blocky crystals in the C28 sample.

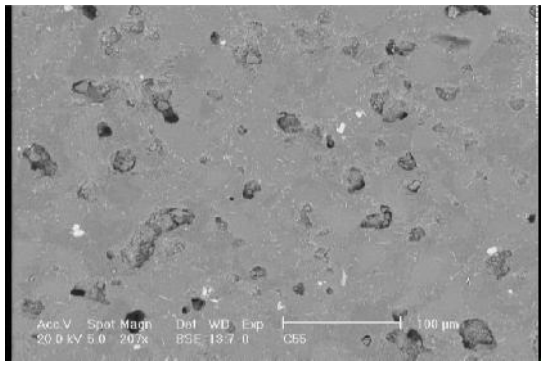

Figure 7. SEM micrograph of the C55 sample sintered at 1050˚C for 1 hr

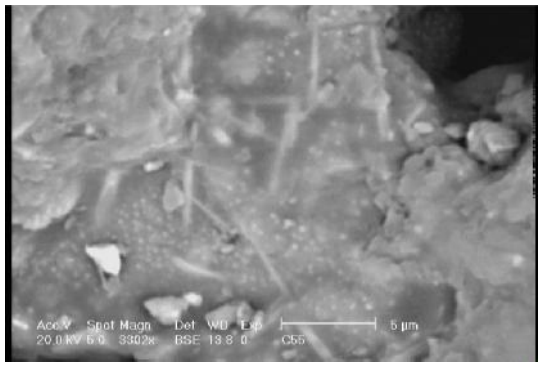

Figure 8. SEM micrograph of the C55 sample sintered at 1050°C for 1 hr

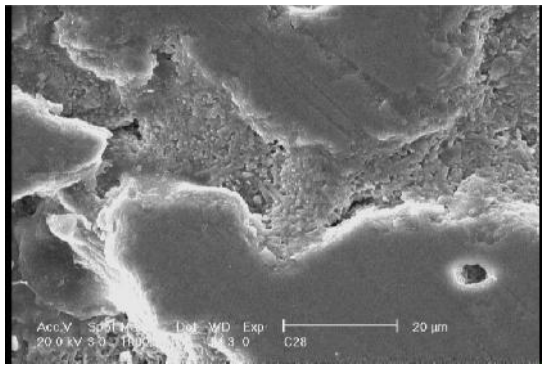

Figure 9. SEM micrograph of the C28 sample sintered at 1160°C for 1 hr

The microstructure of C28 sample would also elucidate the high bending strength, as previously shown in Figure 5. Additionally, Young's modulus, fracture toughness and subsequent bending strength of the C28 sample had the highest values at the lowest hardness.

This behavior indicates (Fig. 10) achieving to a highly interconnected crystalline microstructure.

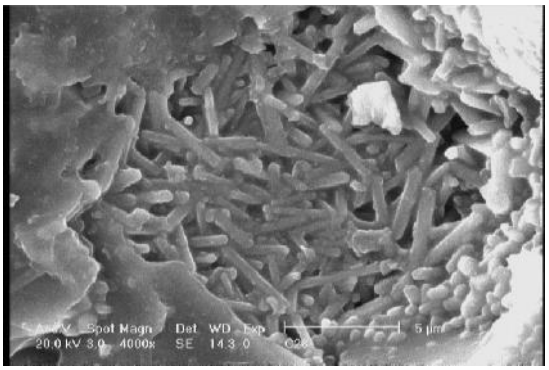

Figure 10. SEM micrograph of the C28 sample sintered at 1160°0C for 1 hr

According to the Figs. 8,10, the rod shape crystals of diopsides were surrounded by the some amorphous like phase in both composites, but the presence of the amorphous phase was more clear in the case of C55 micrograph. In other words, the C55 sample contains more amorphous phases (as mentioned earlier), which is probably led to a low strength. Figure 8 also shows a needle-like microstructure for the C55 compared to the C28. It is possibly due to the lower sintering temperature and lower viscosity, which both are responsible for lower bending strength in the C55 sample.

4. CONCLUSION

The high relative density was difficultly obtained in apatite-wollastonite-phlogopite glass-ceramic. As a result, the bending strength of the composites was influenced by the porosity, which decreased the fracture toughness (81 MPa for bending strength and 1.12 $MPa.m^{1/2}$ for fracture toughness). Consequently, it can be stated that the forsterite as well as the phlogopite phase was led to increase the hardness of the composites. The presence of more amorphous phase in the C28 sample resulted in the blocky diopside grains, which probably increased the bending strength to 107 MPa.

ACKNOWLEDGEMENTS

This work would not have been possible without the financial support of the Merc. I am especially indebted to Mr. Jabbari technician of ceramic division.

REFERENCES

1. Kokubo,T., Shigematsu, M., Nagashima,Y., Tashiro, M., Apatite- and Wollastonite-containing glass-ceramic for prosthetic application. ***Bulletin of the Institute for Chemical Research,*** Kyoto University Vol. 60 ,(1982), 260–268.
2. 2. Yamamuro, T., A–W glass-ceramic: clinical applications. In An introduction to bioceramics, L.L. Hench and J. Wilson, Editors, Eds., ***World Scientific***, Singapore (1993), p 89–104.
3. Yamamuro, T., A–W glass-ceramic in spinal repair. In: J. Wilson, L.L. Hench and D.C. Greenspan, Editors, ***Bioceramics,*** Vol. 8, Elsevier Science Ltd, Oxford (1995), 123–127.
4. 4. Yamamuro ,T., Reconstruction of the iliac crest with bioactive glass-ceramic prostheses. In: T. Yamamuro, L.L. Hench and J. Wilson, Editors, ***Handbook of bioactive ceramics,*** bioactive glasses and glass-ceramic Vol. 1, CRC Press, Boca Raton (1990), 335–342.
5. Hench, L., Ethridge EC. In: Biomaterials: an interfacial approach, ***biophysics and bioengineering***, Series 4. New York: Academic Press; 1982. 2–86 [Chapter 5].
6. Liu. D.M. and Chou. H.M., Formation of a new bioactive glass-ceramic***. Journal of Materials Science: Materials in Medicine***, Vol. 5 (1994), 7–10.
7. Kokubo .T , Bioactive glass-ceramics: properties and applications. ***Biomaterials,*** Vol. 12, (1991), 155–163.
8. Ravaglioli, A., Krajewski, A. and Portu, G. de, Problems involved in assessing mechanical behaviour of bioceramics. In: H. Oonishi, H. Aoki and K. Sawai, Editors, ***Bioceramics,*** Vol. 1, Elsevier Science Ltd, Oxford, (1989), 13–18
9. Pantano, C.G., Clark, E. A., Hench, L.L., Corrosion films on bioglass surfaces, ***Journal of the American Ceramic Society***, Vol. 57, (1974), 412-413.
10. Neo, M., Kotani, S., Fujita, Y., Nakamura, T. Differences in ceramic-bone interface between surface-active ceramics and resorb able ceramics. ***Journal of Biomedical Materials Research***, Vol. 26, (1992), 255-258.
11. Frigge, M., Völksch, G., Investigation of the Bonding Mechanism of Glass Ceramic Layers on Metal Alloys, ***Microchimica Acta*** ,Vol.13, (1996), 299-305
12. Hoche.T. Cornelia, C., Moisescu, I., Microstructure of SiO2-Al2O3-CaO-P2O5-K2O-F-Glass Ceramics. 1. Needlelike versus Isometric Morphology of Apatite Crystals, ***Chemistry of Materials***.,Vol. 13,(2001), 1312-1319
13. Dimitrova-Lukacs, M., Lukacs, P., et al, Silicates Industries, Vol.11, (1996), 15-20
14. Cooper, R.F. Chyung, K., Structure and chemistry of fiber marix interface in Sic fiber reinforced glass-ceramics Composite, ***Journal of Materials Scienc***, Vol. 22 ,(1987), 3148-3160
15. Saori, S., Mechanical properties of spinel /mica composites, ***Journal of the European Ceramic Society***,Vol,108,No.2, (2000), 1079-1084
16. Rabinovich,E.M, Preparation of glass by sintering, ***Journal of Materials Science***, Vol. 20, (1985), 4259-61
17. Juhasz,J. A., Best. S. M., Brooks. R., Kawashita, M., Miyata, N, "Mechanical properties of glass-ceramic, A–W-polyethylene composites: effect of filler content and particle size" ***Biomaterials***, Vol. 25, No 6, (2004), 949-955
18. Faeghi-Nia, A., Preparation of Apatite-Wollastonite-Phlogopite Glass-Ceramic Composites by Powder Sintering Method, ***Science of Sintering***, Vol.45,(2013) ,331-339
19. 19. Faeghi-Nia, A., Marghussian.V., Taheri-Nassaj, E.,Pressureless Sintering of Apatite/Wollastonite–Phlogopite Glass–Ceramics, ***Journal of the American Ceramic Society*** ,Vol.92, No.7, (2009), 1514-1518
20. Faeghinia. A., Shahgoli.N and Jabbari.E, Phlogopite glass-ceramic coatings on stainless steel substrate by plasma spray, ***Advanced Ceramics Progress***, Vol. 2, No. 2, (2016), 16-21
21. 21. Faeghi-Nia, A., Marghussian,V., Taheri-Nassaj, E., Effect of B2O3 on crystallization behavior and microstructure of MgO–SiO2–Al2O3–K2O–F glass–ceramics. ***Ceramics International***, Vol. 33, No. 5, (2007), 773–778.